Int. J. Electrochem. Sci., 17 **(2022)** Article Number: 220672, doi: 10.20964/2022.06.72

International Journal of
ELECTROCHEMICAL
SCIENCE
www.electrochemsci.org

Electrochemical sensor based on Bimetallic phosphosulfide Zn–Ni–P–S Nanocomposite -reduced graphene oxide for determination of Paraoxon Ethyl in agriculture wastewater

BoAn Xiao

Zhengzhou Preschool Education College, Zhengzhou 450000, China
E-mail: mjmj0815123@sina.com

Received: 24 February 2022 / *Accepted:* 26 April 2022 / *Published:* 7 May 2022

This research focused on the development of an electrochemical sensor for the detection of paraoxon ethyl (POE) in agricultural wastewater using a bimetallic phosphosulfide Zn–Ni–P–S nanocomposite-reduced graphene oxide modified glassy carbon electrode (Zn–Ni–P–S/GO/GCE). The hydrothermal process was used to make the nanocomposite. SEM and XRD investigations revealed that the Zn–Ni–P–S/GO nanocomposites were successfully prepared. The limit of detection and sensitivity were estimated to be 35 nM and 0.06369 μA/μM, respectively, in electrochemical studies using DPV and amperometry analyses, and a wide linear range response to POE (1 to 200 μM) was observed on the Zn–Ni–P–S/GO/GCE surface compared to other reported paraoxon sensors in the literature, which was associated with the incorporation of high conductive Zn–Ni bimetallic phosphosulf Bimetallic-based nanoparticles acted as a bridge between the GO and GCE surfaces, facilitating charge transfer. The proposed sensor was successfully applied to the determination of POE pesticide in agricultural wastewaters, with results indicating that the obtained recovery (90.00 to 98.00%) and RSD (2.32 to 4.37%) values by the standard addition method indicate that the proposed method for determining POE in agricultural wastewaters has good accuracy and precision.

Keywords: Electrochemical Sensor; Bimetallic phosphosulfide Zn–Ni–P–S; Nanocomposite, hydrothermal; Silver Nanoparticles; Graphene Oxide; Paraoxon Ethyl; agricultural wastewaters

1. INTRODUCTION

The aryl dialkyl phosphate paraoxon-ethyl (POE; Diethyl p-nitrophenyl phosphate) has both alkyl and aryl groups that are ethyl and the aryl group is 4-nitrophenyl. POE is a very unstable parasympathomimetic that is also extremely poisonous [1-3]. Because of the active metabolite of the insecticide parathion, it can operate as a cholinesterase inhibitor and be employed as a pesticide [4-6]. Scientists have used POE to investigate the acute and chronic effects of organophosphate poisoning [7-

9]. According to reports, it is easily absorbed via the skin, and POE exposure produces an increase in cholinergic activity and glutamate release, which can result in seizures, excitotoxicity, and brain damage [10-12]. Thus, detection of POE is very important and many studies have been conducted on the design and optimization of the Paraoxon sensor [13-15] using chemiluminescent flow sensors [16, 17], flow-injection [18] fluorometry [19], and electrochemical techniques [14, 20, 21]. Among these methods, electrochemical techniques have been shown to have fast, low-cost, and sensitive performance, and the ability to modify the electrode surface in electrochemical methods can improve the efficiency and sensing characteristics of POE sensors [22-24]. However, finding the appropriate composition to improve the detection limit and liner range of the sensor is an important factor for application in fruits, vegetables, environmental and wastewaters samples. Therefore, this study was conducted on the synthesis of Zn–Ni–P–S and Zn–Ni–P–S/GO nanocomposites modified by GCE for the detection of POE in agricultural wastewaters.

2. EXPERIMENTAL

2.1. Preparation of Zn–Ni–P–S/GO nanocomposite modified electrode

The hydrothermal method was used to create the bimetallic phosphosulfide Zn–Ni–P–S nanocomposite [25]: 0.6 mM $Zn(NO_3)_2$•$6H_2O$ (99%, Sigma-Aldrich), 1.2 mM of $Ni(NO_3)_2$•$6H_2O$ (99%, Merck, Germany), 0.6 mM of NH_4F (≥98.0%, Sigma-Aldrich) and 17 mM of $(NH_2)_2CO$ (99%, Sigma-Aldrich) solutions were ultrasonically mixed in 50 mL of deionized water for 20 minutes. Then, for one hour at room temperature, a piece of cleaned Ni foam (1 cm2, Sigma-Aldrich) supported precursor was immersed in the combined solution. The resulting mixture was then transferred to a Teflonlined stainless steel autoclave with a capacity of 100mL and sealed. For five hours, the autoclave was kept at 125°C. The Ni foam with loaded products was washed and dried at 40 °C for 10 hours before being placed in the center of a tube furnace, with NaH_2PO_2•H_2O (99.0%, Sigma-Aldrich) and thiourea (99.0%, Sigma-Aldrich) with a mass ratio of 2:1:4 placed on the adjacent side 3 cm upstream from the Zn-Ni-Precursor. Afterward, the reaction was carried out using an Ar atmosphere at a flow rate of 60 sccm at 400 °C for 120 minutes. After cooling, Zn–Ni–P–S nanocomposite was obtained. For synthesis of the Zn–Ni–P–S/GO Nanocomposite, 400 mg of Zn–Ni–P–S powder was ultrasonically mixed with 15 ml of 6 g/l GO suspension (99%, Luoyang Tongrun Info Technology Co., Ltd., China). Thereupon, the obtained suspension was transferred into the 100 ml Teflon-lined stainless steel autoclave at 250°C for 8 hours. After hydrothermal reactions, the resultant precipitates were washed several times with deionized water and ethanol, and 5 mL of the obtained Zn–Ni–P–S/GO nanocomposite was dropped on the GCE surface, and dried in the oven at 85 °C for 8 hours.

2.2. Preparation actual sample

The agricultural wastewater used in this study was taken from the Wangyang River in Hebei Province, North China, to prepare the real sample. The wastewater was used without any filtration and

was used to make 0.1 PBS (pH 7.4), which was then mixed in an equal volume ratio with 2M POE solution.

2.3. Characterization devices

Scanning electron microscopy (SEM; JEOL FE 7000, JEOL, Tokyo, Japan) and X-ray diffraction (XRD; Rigaku, D/max-A Xray diffractometer, with Cu- radiation) were used to characterize the surface morphology and crystal structure of nanocomposites. Electrochemical properties of the modified electrode were investigated by DPV and amperometry techniques using potentiostat-galvanostat (PGSTAT model 204 equipped with a module FRA32 M, Metrohm Autolab, Utrecht, The Netherlands) in a conventional electrochemical cell which consisted of modified GCE as a working electrode, platinum plate as a counter, and Ag/AgCl as a reference electrode in 0.1 M phosphate buffer solution (PBS, Sigma-Aldrich) with pH 7.4.

3. RESULTS AND DISCUSSION

3.1. Studies of surface morphology and crystal structure

SEM images of surface morphology Zn–Ni–P–S and Zn–Ni–P–S/GO nanocomposites modified GCE are shown in Figures 1a and 1b. Zn–Ni–P–S nanoparticles of spherical shape with an average diameter of 55 nm are scattered throughout the framework, as seen in the SEM picture of Zn–Ni–P–S.

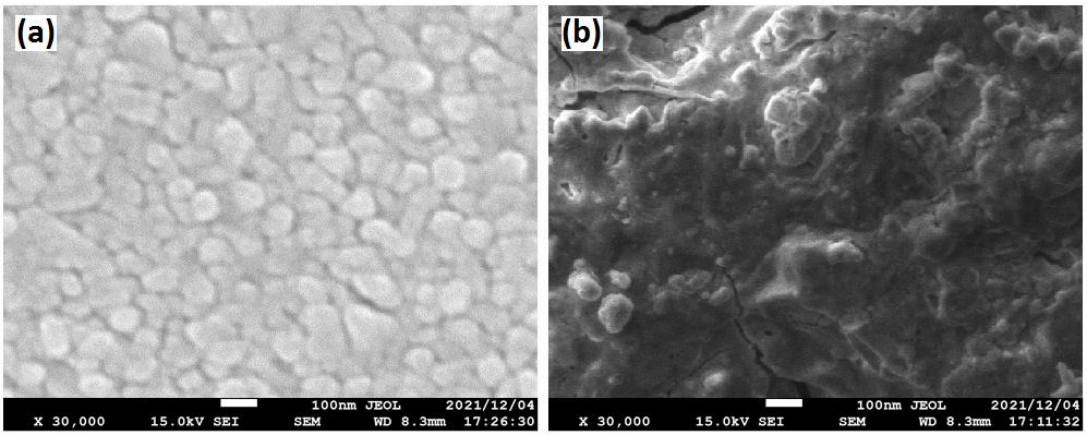

Figure 1. SEM images of surface morphology (a) Zn–Ni–P–S and (b) Zn–Ni–P–S/GO nanocomposites modified GCE.

In Figure 1b, a considerable number of Zn–Ni–P–S nanoparticles are uniformly spread over GO nanosheets in a SEM picture of Zn–Ni–P–S/GO nanocomposite. A considerable amount of Zn–Ni–P–S in a spherical shape is uniformly distributed on the GO sheets, and the porous morphology and

increased effective surface area of Zn–Ni–P–S/GO nanocomposite modified GCE are achieved, which promote analyte absorption and electrode sensitivity. P and S, as well as transition metals, have been shown to interact in studies. P and S, as well as transition metals Zn and Ni, have been shown in studies to interact with the GO sheets via physisorption, electrostatic binding, or charge-transfer interactions [26-28]. The average diameter of Zn–Ni–P–S on GO sheets is also 55 nm.

The results of XRD analyses of powders of Zn–Ni–P–S and Zn–Ni–P–S/GO nanocomposites are shown in Figure 2. The XRD pattern of Zn–Ni–P–S shows two distinct diffraction peaks at 44.55° and 52.21°, which correspond to Ni diffraction planes (111) and (200) (JCPDS card no. 04-0850) [29-31], as well as a diffraction peak at 40.81°, which corresponds to Ni2P diffraction plane (111). (CPDS card no. 03-0953). Furthermore, the diffraction peaks at 21.51°, 31.16°, 37.91°, 50.22°, and 55.30° correspond to the Ni3S2 planes (010), (110), (111), (120), and (121). (CPDS card no. 85-1802) [32-34]. The XRD pattern of Zn–Ni–P–S/GO nanocomposites demonstrates the additional diffraction peaks at 10.65°, corresponding to the diffraction plane of (001) of GO. Hence, the results of SEM and XRD analyses indicate the successful preparation of Zn–Ni–P–S/GO nanocomposites using the hydrothermal method.

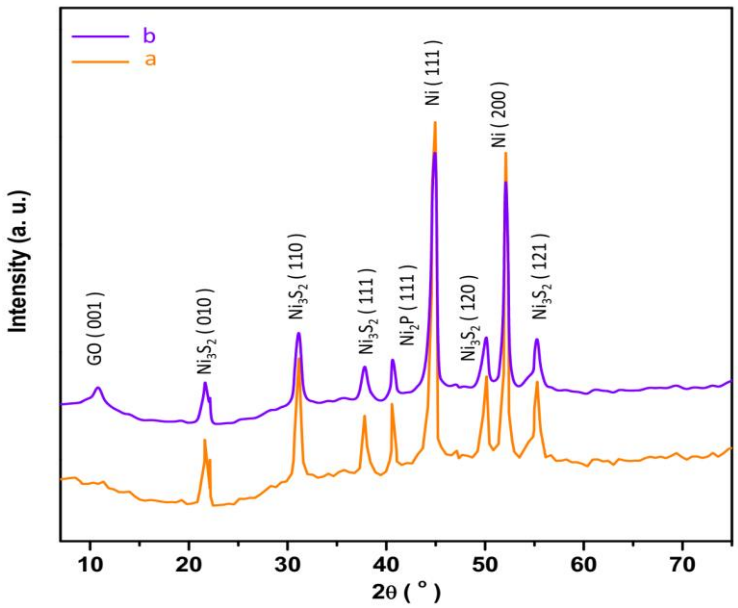

Figure 2. XRD analyses of powders of (a) Zn–Ni–P–S and (b) Zn–Ni–P–S/GO nanocomposites.

3.2. Electrochemical Studies

Figure 3 shows the results of DPV studies of GCE, Zn–Ni–P–S/GCE, and Zn–Ni–P–S/GO/GCE in 0.1 M PBS (pH 7.4) in the absence and presence of 40 µM POE at a scan rate of 30 mV/s in the absence and presence of 40 M POE. In the absence of 40 M POE, no redox peak can be seen on any of the electrodes. The DPV curves of GCE, Zn–Ni–P–S/GCE, and Zn–Ni–P–S/GO/GCE show an oxidation peak of POE at 0.42 V, 0.41 V, and 0.39 V, respectively, in the presence of 40 M POE. It is has been found that the electrochemical mechanism contains of four electrons and four

protons and is accompanied by the reduction of the nitro-group (–NO2) to the hydroxylamine (–NHOH) group (equation 1, Figure 4), and a two-electron transfer process (equation 2, Figure 4) [20, 35, 36].

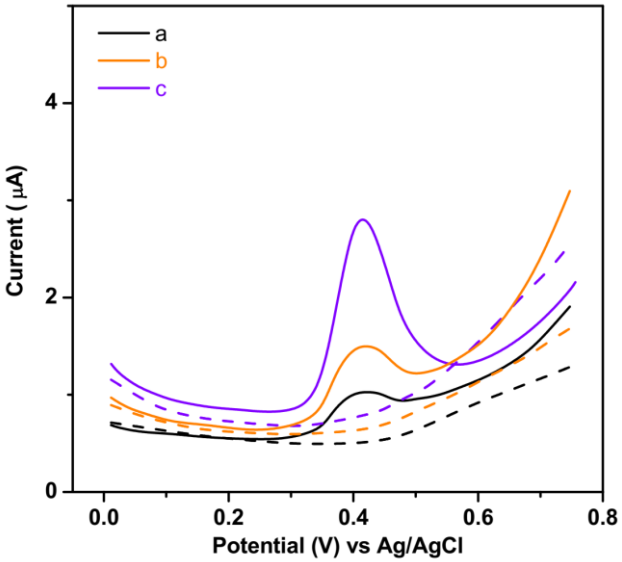

Figure 3. Results of DPV analyses of (a) GCE, (b) Zn–Ni–P–S/GCE and (c) Zn–Ni–P–S/GO/GCE in 0.1 M PBS (pH 7.4) in absence (dashed line) and presence (solid line) of 40 µM POE at scan rate of 30mV/s.

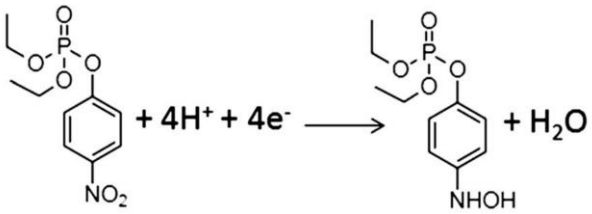

(1)

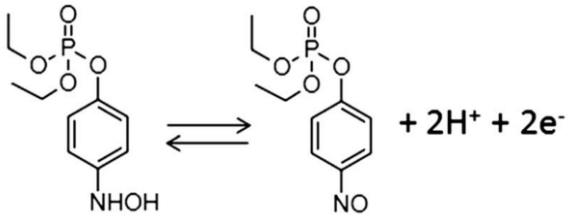

(2)

Figure 4. Schematic image of the POE electrochemical mechanism.

The lower potential and higher current response to POE on the Zn–Ni–P–S/GO/GCE surface are associated with the larger specific surface area, higher porosity, and electrical conductivity of GO nanosheets and Zn–Ni bimetallic phosphosulfide nanocomposite, according to the anodic peak current of electrodes. Many oxygen-containing functional groups on GO provide various active sites for analyte molecule uptake [37-39]. Moreover, the morphology and chemical composition of Zn–Ni–P–

S/GO/GCE such as π-conjugative structure show high adsorptive capacities adsorbing sensing layers that provide more charge carriers and ion transport pathways and can facilitate electron transfer in the sensing mechanism [40-42]. The resulted nanocomposite can act as a favorable electrochemical structure with sufficient channels for ions migration in electrochemical reactions [43, 44]. Therefore, the synergetic effect of Zn–Ni bimetallic phosphosulfide nanocomposite and GO nanosheets promotes the electrochemical response and decreases the electrochemical reaction potential.

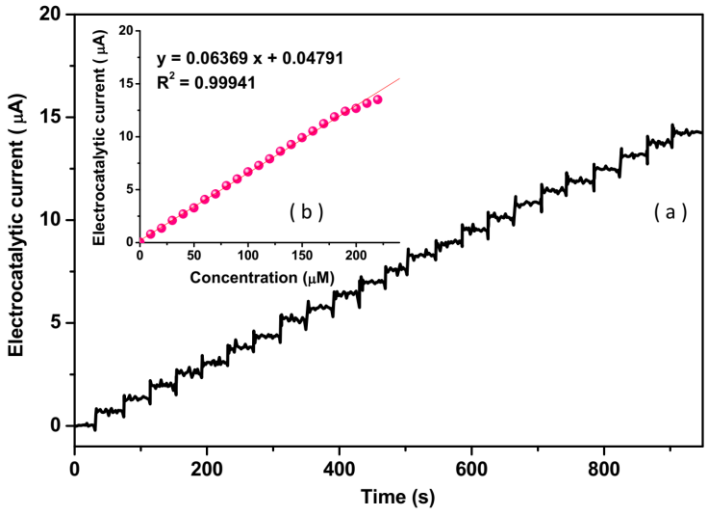

Figure 5. Amperometric response and calibration graph of Zn–Ni–P–S/GO/GCE during the successive addition of POE at regular intervals of 40 s into 0.1 M PBS (pH 7.4) at potential of 0.39 V.

Figure 5 depicts the amperometric response and calibration graph of Zn–Ni–P–S/GO/GCE in 0.1 M PBS (pH 7.4) with the addition of POE at a potential of 0.39 V at regular intervals of 40 s. The electrocatalytic reaction of Zn–Ni–P–S/GO/GCE is shown to be quick following each addition of POE solution [45-47]. With a correlation coefficient of 0.99941, the electrocatalytic current increases linearly with increasing POE concentration in the range of 1 to 200 μM, as shown in Figure 5b. The linear relationship is achieved as [48, 49]:

$$I\ (\mu A) = 0.06369\ [POE]\ (\mu A/\mu M) + 0.04791 \quad (3)$$

Where [POE] is the POE concentration. The values of limit of detection (LOD) and sensitivity are estimated to be 35 nM and 0.06369μA/μM, respectively. Table 1 shows the comparison between the sensing performance of the POE sensor in this work and the other reported Paraoxon sensors in the literature, indicating a wide linear range response to the POE, and comparable or better performance of Zn–Ni–P–S/GO/GCE than the other reported Paraoxon sensors which can be attributed to excellent charge transfer kinetics, the great active sites on both basal and edge structural defects on GO sheets [50-53]. It demonstrates that the incorporation of high conductive Zn–Ni bimetallic phosphosulfide nanocomposite between GO nanosheets improves the electrocatalytic response. Bimetallic based nanoparticles provide a bridge effect between the GO and GCE surface and promote charge transfer rates [54-56].

Table 1. Comparison between sensing performance of POE sensor in this work and the other reported Paraoxon sensors in the literature.

Electrode	Technique	LOD (nM)	Linear range (µM)	Ref.
Zn–Ni–P–S/GO/GCE	AMP	35	1−200	This work
$BiVO_4$ nano dendrites	CV	30	20–100	[20]
CdTe/ZnS QDs/GCE	CV	1.72	1.2×10^{-4}–0.061	[57]
Nd-UiO-66@MWCNT	DPV	0.04	7×10^{-4}–0.1	[58]
CeO_2/GCE	DPV	60	0.1–100	[59]
$NiCo_2O_4$	SWV	80	----	[60]
CuNCs@BSASWCNT	SWV	12.8	0.05–35	[61]
TiO_2@dopamine@serine/histamine/glutamic acid	SWV	200	0.5–100	[62]

AMP: Amperometry; CV: Cyclic Voltammetry; SWV: Square wave voltammetry

Table 2. Results of interference studies of Zn–Ni–P–S/GO/GCE to determination POE using amperometric experiments in 0.1 M PBS (pH 7.4) at potential of 0.39 V in presence of most commonly found compounds in real samples of vegetables and agricultural wastewaters.

Substance	Added (µM)	Amperometric signal (µA) at 0.39 V	RSD (%)
POE	1	0.0637	±0.0022
Malathion	3	0.0062	±0.0009
Chlorfenvinphos	3	0.0041	±0.0011
Fensulfothion	3	0.0031	±0.0008
Chlorpyrifos	3	0.0041	±0.0009
Carbofuran	3	0.0015	±0.0004
Uric acid	3	0.0088	±0.0008
Cr^{2+}	3	0.0089	±0.0007
Cu^{2+}	3	0.0026	±0.0009
K^+	3	0.0032	±0.0007
Na^+	3	0.0024	±0.0003
SO_4^{2-}	3	0.0037	±0.0007
Mn^{2+}	3	0.0015	±0.0003
Li^{2+}	3	0.0029	±0.0004
Pb^{2+}	3	0.0039	±0.0005
Hg^{2+}	3	0.0028	±0.0003
Ni^{2+}	3	0.0053	±0.0003
Fe^{2+}	3	0.0057	±0.0008
Cl^-	3	0.0065	±0.0005

Table 2 shows the findings of interference studies of Zn–Ni–P–S/GO/GCE to determine POE using amperometric experiments in 0.1 M PBS (pH 7.4) at a potential of 0.39 V using amperometric measurements in 0.1 M PBS (pH 7.4) at a potential of 0.39 V. These tests included looking at the

suggested electrode's amperometric response for determining POE and the 3-fold of the most often observed chemicals in real samples of vegetables and agricultural wastewaters [59, 63]. Findings show that additional interference compounds have a minimal reaction, that the sensor's sensitivity to POE is significantly greater than that of the interfering species, and that addition interference compounds have a negligible response [64-66]. As a result, the compounds listed in Table 2 have no effect on POE determination, and the proposed electrode might be employed as a quick and precise POE sensor [67, 68].

The practical application of Zn–Ni–P–S/GO/GCE to determine the POE pesticide in agricultural wastewaters was investigated. The concentrations of POE were estimated in a prepared real sample of agricultural wastewater using amperometric experiments in 0.1 M PBS (pH 7.4) at a potential of 0.39 V with the addition of POE solutions [69, 70]. The amperometric measurements and resultant calibration graph of a prepared genuine sample of agricultural wastewater are shown in Figure 6. As can be shown, the POE concentration in electrochemical cells of prepared sample in 0.1M PBS is 1.03 M, indicating a POE content of 0.03 M in genuine agricultural wastewater samples. Additionally, Table 3 shows that the obtained recovery (90.00 to 98.00%) and RSD (2.32 to 4.37%) values by the standard addition method, indicate good accuracy and high precision of the proposed method for determination of the POE in agricultural wastewaters [71, 72].

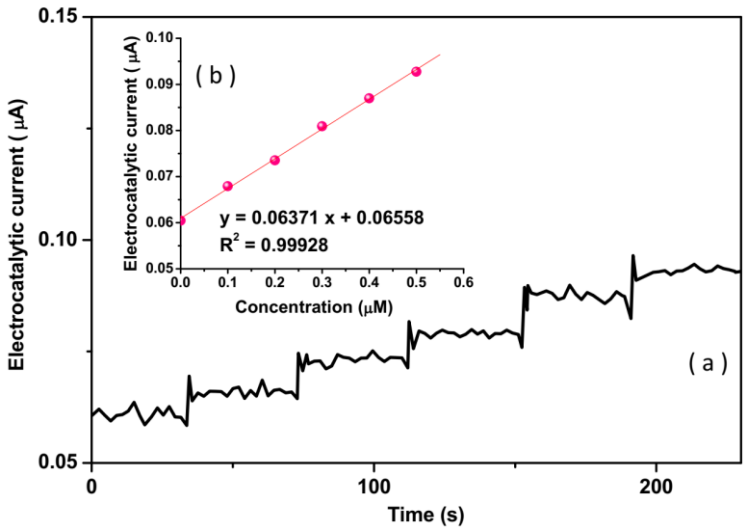

Figure 6. Amperometric response and calibration graph of Zn–Ni–P–S/GO/GCE during the successive addition of POE at regular intervals of 40 s into the prepared 0.1 M PBS (pH 7.4) real samples of agricultural wastewater at potential of 0.39 V.

Table 3. The analytical findings of determination of POE in the agricultural wastewater sample.

added (μM)	Found (μM)	Recovery (%)	RSD (%)
0.10	0.09	90.00	2.32
0.20	0.19	95.00	4.37
0.30	0.28	93.33	3.29
0.40	0.39	97.50	4.14
0.50	0.49	98.00	3.17

4. CONCLUSION

In conclusion, the fabrication of an electrochemical sensor based on (Zn–Ni–P–S/GO/GCE for the measurement of POE in agricultural wastewater was given in this study. The hydrothermal technique was used to make the Zn–Ni–P–S/GO nanocomposite. The structural results confirmed that the Zn–Ni–P–S/GO nanocomposites were successfully produced. Electrochemical investigations revealed that the limit of detection and sensitivity were calculated to be 35 nM and 0.06369 A/M, respectively, and that a wide linear range response to POE (1 to 200 M) was observed on the Zn–Ni–P–S/GO/GCE surface compared to other previously reported Paraoxon sensors. The proposed sensor was successfully used to determine the POE pesticide in an agricultural wastewater sample, and the results showed that the standard addition method obtained recovery (90.00 to 98.00 percent) and RSD (2.32 to 4.37 percent) values, indicating that the proposed method for determining the POE in agricultural wastewaters is accurate and precise.

References

1. B. Gökçe, N. Sarıoğlu, N. Gençer and O. Arslan, *Journal of Biochemical and Molecular Toxicology*, 33 (2019) e22407.
2. H. Karimi-Maleh, C. Karaman, O. Karaman, F. Karimi, Y. Vasseghian, L. Fu, M. Baghayeri, J. Rouhi, P. Senthil Kumar and P.-L. Show, *Journal of Nanostructure in Chemistry*, (2022) 1.
3. T. Zhang, X. Wu, S.M. Shaheen, H. Abdelrahman, E.F. Ali, N.S. Bolan, Y.S. Ok, G. Li, D.C. Tsang and J. Rinklebe, *Journal of hazardous materials*, 425 (2022) 127906.
4. L. Jin, Z. Hao, Q. Zheng, H. Chen, L. Zhu, C. Wang, X. Liu and C. Lu, *Analytica Chimica Acta*, 1100 (2020) 215.
5. L. Zhang, Y. Xu, H. Liu, Y. Li, S. You, J. Zhao and J. Zhang, *Journal of Water Process Engineering*, 44 (2021) 102368.
6. J. Rouhi, S. Mahmud, S.D. Hutagalung and N. Naderi, *Electronics letters*, 48 (2012) 712.
7. P. Houzé, A. Hutin, M. Lejay and F.J. Baud, *Toxics*, 7 (2019) 23.
8. W. Liu, F. Huang, Y. Liao, J. Zhang, G. Ren, Z. Zhuang, J. Zhen, Z. Lin and C. Wang, *Angewandte Chemie*, 120 (2008) 5701.
9. L. He, C. Yang, J. Ding, M.-Y. Lu, C.-X. Chen, G.-Y. Wang, J.-Q. Jiang, L. Ding, G.-S. Liu and N.-Q. Ren, *Applied Catalysis B: Environmental*, 303 (2022) 120880.
10. K.L. Farizatto and B.A. Bahr, *European scientific journal*, 13 (2017) 29.
11. H. Karimi-Maleh, H. Beitollahi, P.S. Kumar, S. Tajik, P.M. Jahani, F. Karimi, C. Karaman, Y. Vasseghian, M. Baghayeri and J. Rouhi, *Food and Chemical Toxicology*, (2022) 112961.
12. Z. Zhang, Y. Lou, C. Guo, Q. Jia, Y. Song, J.-Y. Tian, S. Zhang, M. Wang, L. He and M. Du, *Trends in Food Science & Technology*, 118 (2021) 569.
13. X. Zhang, Y. Feng, J. Li, D. Ai, G. Xi and M. Zhao, *International Journal of Electrochemical Science*, 16 (2021)
14. G. Zhao, H. Wang and G. Liu, *International Journal of Electrochemical Science*, 10 (2015) 9790.
15. M. Pohanka, M. Hrabinova, J. Fusek, D. Hynek, V. Adam, J. Hubalek and R. Kizek, *International Journal of Electrochemical Science*, 7 (2012) 50.
16. A. Roda, P. Rauch, E. Ferri, S. Girotti, S. Ghini, G. Carrea and R. Bovara, *Analytica Chimica Acta*, 294 (1994) 35.
17. Y. Chu and T. Zhao, *Mathematical Inequalities & Applications*, 19 (2016) 589.
18. M. Leon-Gonzalez and A. Townshend, *Analytica Chimica Acta*, 236 (1990) 267.

19. N. Kamelipour, A. Mohsenifar, M. Tabatabaei, T. Rahmani-Cherati, K. Khoshnevisan, A. Allameh, M.M. Milani, S. Najavand and B. Etemadikia, *Microchimica Acta*, 181 (2014) 239.
20. P.K. Gopi, D.B. Ngo, S.-M. Chen, C.H. Ravikumar and W. Surareungchai, *Chemosphere*, 288 (2022) 132511.
21. C.-X. Chen, S.-S. Yang, J. Ding, G.-Y. Wang, L. Zhong, S.-Y. Zhao, Y.-N. Zang, J.-Q. Jiang, L. Ding and Y. Zhao, *Applied Catalysis B: Environmental*, 298 (2021) 120495.
22. Y. Luo, Y. Xie, H. Jiang, Y. Chen, L. Zhang, X. Sheng, D. Xie, H. Wu and Y. Mei, *Chemical Engineering Journal*, 420 (2021) 130466.
23. T.-H. Zhao, Z.-Y. He and Y.-M. Chu, *AIMS Mathematics*, 5 (2020) 6479.
24. K. Eswar, J. Rouhi, H. Husairi, M. Rusop and S. Abdullah, *Advances in Materials Science and Engineering*, 2014 (2014) 1.
25. X. Lei, S. Ge, Y. Tan, J. Li, Z. Wang, P. Liu, C. Feng and B. Xiang, *Journal of Materials Chemistry A*, 7 (2019) 24908.
26. A. Anouar, A. Grirrane, E. Álvarez, N. Katir, A. Primo, H. Garcia and A. El Kadib, *Materials Today Sustainability*, 18 (2022) 100109.
27. B. Zhu, K. Wang, W. Sun, Z. Fu, H. Ahmad, M. Fan and H. Gao, *Composites Science and Technology*, 218 (2022) 109209.
28. W. Liu, J. Li, J. Zheng, Y. Song, Z. Shi, Z. Lin and L. Chai, *Environmental Science & Technology*, 54 (2020) 11971.
29. A.R. Ridzuan, S. Ibrahim, S. Karman, M.S. Ab Karim, W.S.W.K. Zaman and C.C. Khuen, *International Journal of Electrochemical Science*, 16 (2021) 210557.
30. H. Karimi-Maleh, R. Darabi, M. Shabani-Nooshabadi, M. Baghayeri, F. Karimi, J. Rouhi, M. Alizadeh, O. Karaman, Y. Vasseghian and C. Karaman, *Food and Chemical Toxicology*, 162 (2022) 112907.
31. F. Husairi, J. Rouhi, K. Eswar, C.R. Ooi, M. Rusop and S. Abdullah, *Sensors and Actuators A: Physical*, 236 (2015) 11.
32. O.S. Onwuka, C.K. Ezugwu and S.I. Ifediegwu, *Geology, Ecology, and Landscapes*, 3 (2019) 65.
33. H.-H. Chu, T.-H. Zhao and Y.-M. Chu, *Mathematica Slovaca*, 70 (2020) 1097.
34. S.A. Iqbal, M.G. Hafez, Y.-M. Chu and C. Park, *Journal of Applied Analysis & Computation*, 12 (2022) 770.
35. D. Sharma and K.D. Yadav, *Malaysian Journal of Sustainable Agriculture (MJSA)*, 1 (2017) 15.
36. K.A. Zahidah, S. Kakooei, M. Kermanioryani, H. Mohebbi, M.C. Ismail and P.B. Raja, *International Journal of Engineering and Technology Innovation*, 7 (2017) 243.
37. Q. Wu, Y. Sun, P. Ma, D. Zhang, S. Li, X. Wang and D. Song, *Analytica Chimica Acta*, 913 (2016) 137.
38. M.-K. Wang, M.-Y. Hong, Y.-F. Xu, Z.-H. Shen and Y.-M. Chu, *Journal of Mathematical Inequalities*, 14 (2020) 1.
39. R. Mohamed, J. Rouhi, M.F. Malek and A.S. Ismail, *International Journal of Electrochemical Science*, 11 (2016) 2197.
40. H. Zhong, M. Wang, G. Chen, R. Dong and X. Feng, *ACS Nano*, 16 (2022) 1759.
41. Q. Dai, K. Shen, W. Deng, Y. Cai, J. Yan, J. Wu, L. Guo, R. Liu, X. Wang and W. Zhan, *Environmental Science & Technology*, 55 (2021) 4007.
42. Y.-M. Chu, B. Shankaralingappa, B. Gireesha, F. Alzahrani, M.I. Khan and S.U. Khan, *Applied Mathematics and Computation*, 419 (2022) 126883.
43. G. Wang, D. Huang, M. Cheng, S. Chen, G. Zhang, L. Lei, Y. Chen, L. Du, R. Li and Y. Liu, *Coordination Chemistry Reviews*, 460 (2022) 214467.
44. H. Maleh, M. Alizadeh, F. Karimi, M. Baghayeri, L. Fu, J. Rouhi, C. Karaman, O. Karaman and R. Boukherroub, *Chemosphere*, (2021) 132928.

45. C. Xin, L. Changhe, D. Wenfeng, C. Yun, M. Cong, X. Xuefeng, L. Bo, W. Dazhong, H.N. LI and Y. ZHANG, *Chinese Journal of Aeronautics*, (2021) 1.
46. F. Wang, M.N. Khan, I. Ahmad, H. Ahmad, H. Abu-Zinadah and Y.-M. Chu, *Fractals*, 30 (2022) 2240051.
47. J. Rouhi, S. Kakooei, S.M. Sadeghzadeh, O. Rouhi and R. Karimzadeh, *Journal of Solid State Electrochemistry*, 24 (2020) 1599.
48. T. Gao, C. Li, Y. Zhang, M. Yang, D. Jia, T. Jin, Y. Hou and R. Li, *Tribology International*, 131 (2019) 51.
49. T.-H. Zha, O. Castillo, H. Jahanshahi, A. Yusuf, M.O. Alassafi, F.E. Alsaadi and Y.-M. Chu, *Applied and Computational Mathematics*, 20 (2021)
50. S. Ren, R. Feng, S. Cheng, L. Huang, Q. Wang and Z. Zheng, *Microchemical Journal*, 175 (2022) 107129.
51. S. Guo, C. Li, Y. Zhang, Y. Wang, B. Li, M. Yang, X. Zhang and G. Liu, *Journal of Cleaner Production*, 140 (2017) 1060.
52. S. Rashid, S. Sultana, Y. Karaca, A. Khalid and Y.-M. Chu, *Fractals*, 30 (2022) 2240026.
53. N. Naderi, M. Hashim, J. Rouhi and H. Mahmodi, *Materials science in semiconductor processing*, 16 (2013) 542.
54. B. Shen, H. Huang, Y. Jiang, Y. Xue and H. He, *Electrochimica Acta*, 407 (2022) 139913.
55. M. Nazeer, F. Hussain, M.I. Khan, E.R. El-Zahar, Y.-M. Chu and M. Malik, *Applied Mathematics and Computation*, 420 (2022) 126868.
56. F. Jin, Z.-S. Qian, Y.-M. Chu and M. ur Rahman, *Journal of Applied Analysis & Computation*, 12 (2022) 790.
57. L. Dewangan, J. Korram, I. Karbhal, R. Nagwanshi, K.K. Ghosh, S. Pervez and M.L. Satnami, *Industrial & Engineering Chemistry Research*, 61 (2022) 3636.
58. H. Khoshsafar, N. Karimian, T.A. Nguyen, H. Fakhri, A. Khanmohammadi, A. Hajian and H. Bagheri, *Chemosphere*, 292 (2022) 133440.
59. Y. Sun, J. Wei, J. Zou, Z. Cheng, Z. Huang, L. Gu, Z. Zhong, S. Li, Y. Wang and P. Li, *Journal of Pharmaceutical Analysis*, 11 (2021) 653.
60. Y. Yang, S. Hao, X. Lei, J. Chen, G. Fang, J. Liu, S. Wang and X. He, *Journal of Hazardous Materials*, 428 (2022) 128262.
61. H. Bagheri, A. Afkhami, H. Khoshsafar, A. Hajian and A. Shahriyari, *Biosensors and Bioelectronics*, 89 (2017) 829.
62. L. Qiu, P. Lv, C. Zhao, X. Feng, G. Fang, J. Liu and S. Wang, *Sensors and actuators B: chemical*, 286 (2019) 386.
63. J. Kaur, D. Bandyopadhyay and P.K. Singh, *Journal of Molecular Liquids*, 347 (2022) 118258.
64. M. Yang, C. Li, Y. Zhang, D. Jia, R. Li, Y. Hou, H. Cao and J. Wang, *Ceramics International*, 45 (2019) 14908.
65. B. Li, C. Li, Y. Zhang, Y. Wang, D. Jia and M. Yang, *Chinese Journal of Aeronautics*, 29 (2016) 1084.
66. T.-H. Zhao, M.-K. Wang, G.-J. Hai and Y.-M. Chu, *Revista de la Real Academia de Ciencias Exactas, Físicas y Naturales. Serie A. Matemáticas*, 116 (2022) 1.
67. S.N. Hajiseyedazizi, M.E. Samei, J. Alzabut and Y.-m. Chu, *Open Mathematics*, 19 (2021) 1378.
68. J. Rouhi, S. Mahmud, S. Hutagalung and S. Kakooei, *Micro & Nano Letters*, 7 (2012) 325.
69. Y. Zhang, H.N. Li, C. Li, C. Huang, H.M. Ali, X. Xu, C. Mao, W. Ding, X. Cui and M. Yang, *Friction*, 10 (2022) 803.
70. M. Liu, C. Li, Y. Zhang, Q. An, M. Yang, T. Gao, C. Mao, B. Liu, H. Cao and X. Xu, *Frontiers of Mechanical Engineering*, 16 (2021) 649.
71. J. Zhang, C. Li, Y. Zhang, M. Yang, D. Jia, G. Liu, Y. Hou, R. Li, N. Zhang and Q. Wu, *Journal of Cleaner Production*, 193 (2018) 236.

72. J. Rouhi, S. Mahmud, S.D. Hutagalung and S. Kakooei, *Journal of Micro/Nanolithography, MEMS, and MOEMS*, 10 (2011) 043002.